Laser and Particle Beams (2004), *22*, 1–7. Printed in the USA.

DOI: 10.1017/S0263034604040054

Coupling of longitudinal and transverse motion of accelerated electrons in laser wakefield acceleration

A.J.W. REITSMA AND D.A. JAROSZYNSKI

Department of Physics, Strathclyde University, Glasgow, United Kingdom

(RECEIVED 00 Xxxxxx 0000; ACCEPTED 00 Xxxxx 0000)

Abstract

The acceleration dynamics of electrons in a laser wakefield accelerator is discussed, in particular the coupling of longitudinal and transverse motion. This coupling effect is important for electrons injected with a velocity below the laser pulse group velocity. It is found that the electron bunch is adiabatically focused during the acceleration and that a finite bunch width contributes to bunch lengthening and growth of energy spread. These results indicate the importance of a small emittance for the injected electron bunch.

Keywords: Beam quality; Electron dynamics; Plasma-based acceleration

1. INTRODUCTION

Plasma-based electron acceleration methods (Esarey *et al.*, 1996) are attractive due to the high accelerating gradients that a plasma can provide: the electric field strength can be 3 to 4 orders of magnitude larger than the maximum value attainable in conventional accelerators (Umstadter *et al.*, 1996). Resonant laser wakefield acceleration (LWFA) is one of such schemes that use the extremely high electric fields of a relativistic plasma wave to accelerate electrons. The basic idea of resonant LWFA (Tajima & Dawson, 1976) is to use the ponderomotive force (light pressure) of a laser pulse with a duration shorter than the plasma period to resonantly drive a high-amplitude plasma wave. The phase velocity of this plasma wave (equal to the group velocity of the laser pulse) is below c, so that electrons can be trapped and accelerated in the wake of the laser pulse. In this article, we describe the acceleration dynamics of electrons in such a plasma wave. After discussing some well-known results on the longitudinal and transverse motion of accelerated electrons (Mora & Amiranoff, 1989; Mora, 1992; Andreev *et al.*, 1996), we present an analysis of the coupling between longitudinal and transverse dynamics and a short discussion of the results.

For the description of the plasma wave we use the quasi-static description (Umstadter *et al.*, 1996) i.e., the scalar and vector potentials (ϕ and $\boldsymbol{A}$) are assumed to depend only on the comoving coordinate $\zeta = z - v_g t$ and the transverse coordinate $\boldsymbol{r}_\perp$, where v_g denotes the group velocity of the laser pulse, which defines the *resonant energy* $\gamma_g mc^2$, $\gamma_g = (1 - v_g^2/c^2)^{-1/2}$. Since the electrons move predominantly in the forward direction (z-direction), the approximation $\boldsymbol{v} \approx v_g \hat{e}_z$ can be used to evaluate the Lorentz force (Panofsky & Wenzel, 1956)

$$\frac{d\boldsymbol{P}_\perp}{dt} \approx -e\boldsymbol{E}_\perp - e\,\frac{v_g}{c}\,\hat{e}_z \times \boldsymbol{B} = e\nabla_\perp\left(\phi - \frac{v_g}{c}A_z\right) \tag{1}$$

$$\frac{dP_z}{dt} \approx -eE_z = e\,\frac{\partial}{\partial\zeta}\left(\phi - \frac{v_g}{c}A_z\right). \tag{2}$$

The approximation is correct if both the forward velocity v_z and the group velocity v_g are close to the speed of light c, but the difference between them is much smaller (of order c/γ_g^2). The equations of motion (1)–(2) can be derived from a Hamiltonian (Reitsma *et al.*, 2001)

$$\mathcal{H} = mc^2(\gamma - \Psi) - v_g P_z \tag{3}$$

Address correspondence and reprint request to: A.J.W. Reitsma, Department of Physics, Strathclyde University, John Anderson Building, 107 Rottenrow, G4 0NG Glasgow, United Kingdom. E-mail: a.reitsma@phys.strath.ac.uk

Q1

for which $(\boldsymbol{r}_\perp, \boldsymbol{P}_\perp)$, and (ζ, P_z) form pairs of conjugate canonical coordinates. The dimensionless quantity Ψ, defined by

$$\Psi = \frac{e\phi}{mc^2} - v_g \frac{eA_z}{mc^3} \tag{4}$$

is the *wakefield potential* that governs the electron dynamics.

2. LONGITUDINAL MOTION

Assuming $|P_\perp| \ll P_z$ (paraxial approximation), it is convenient to expand the Hamiltonian in a Taylor series around $\boldsymbol{r}_\perp = 0$, $\boldsymbol{P}_\perp = 0$. To leading order, this reduces $\mathcal{H}$ to a purely one-dimensional Hamiltonian (Esarey & Pilloff, 1995)

$$\mathcal{H}_0 = mc^2(\gamma_0 - \Psi_0) - v_g P_z \tag{5}$$

with (ζ, P_z) as canonical coordinates. In Eq. (5) the notations $\gamma_0 = (1 + P_z^2/m^2c^2)^{1/2}$ and $\Psi_0(\zeta) = \Psi(\boldsymbol{r}_\perp = 0, \zeta)$ are used. For convenience, the subscript-0 will be suppressed in the remainder of this section.

In the linear wakefield regime, the plasma wave equation reduces to a harmonic oscillator equation (Gorbunov & Kirsanov, 1987)

$$\left(k_p^2 + \frac{d^2}{d\zeta^2}\right)\Psi = k_p^2 \Phi_p. \tag{6}$$

where $k_p^2 = 4\pi ne^2/mc^2$ defines the plasma wave-number k_p, and Φ_p is the dimensionless ponderomotive potential of the laser pulse. The solution in the region behind the driving laser pulse is

$$\Psi(\zeta) = E_0 \cos(k_p\zeta), \quad \frac{\partial\Psi}{\partial\zeta}(\zeta) = -k_p E_0 \sin(k_p\zeta) \tag{7}$$

where E_0 is the dimensionless wakefield amplitude and a particular choice of the wakefield phase has been made (without loss of generality).

The phase space diagram contains 3 types of orbits, as can be seen in Figure 1, which shows the (ζ, γ)-phase space diagram for $E_0 = 1/10$, $\gamma_g = 50$. As seen in Figure 1, there are closed orbits inside the separatrix and open orbits both above and below the separatrix. The orbits below the separatrix describe the motion of electrons that are too slow to be captured in the wave. The orbits above the separatrix correspond to the motion of electrons that are out-running the wave. The orbits inside the separatrix describe the *synchrotron* oscillation of electrons that are trapped inside the wave. The dynamics of high-energy electrons out-running the plasma wave (orbits above separatrix) have been studied by Cheshkov *et al.* (2000) and Chiu *et al.* (2000), in the context of a linear collider based on multi-stage laser wakefield acceleration. In this regime, the transverse and longitudinal motion is effectively decoupled and the analysis is considerably simplified. Instead, in this article, we will analyze the dynamics of electrons injected at relatively low energy from a compact conventional electron source (orbits inside separatrix), for which the coupling of longitudinal and transverse dynamics becomes important.

Stable equilibrium points (O-points) are found at $\zeta = n\lambda_p$, $\gamma = \gamma_g$ and unstable equilibrium points (X-points) at $\zeta = (n + 1/2)\lambda_p$, $\gamma = \gamma_g$ for all $n \in \mathbb{Z}$. For orbits inside the separatrix, one defines the *turning points* by the condition $\partial\mathcal{H}/\partial P_z = d\zeta/dt = 0$: at these points the backward phase slip of the electron changes to forward slip or vice versa. In Figure 1 these points are seen to be at $\gamma = \gamma_g$. Points of minimum and maximum energy, defined by $\partial\mathcal{H}/\partial\zeta = 0$, are found at $\zeta = n\lambda_p/2$ for all $n \in \mathbb{Z}$. The minimum and maximum values of γ on the separatrix are denoted $\gamma_{max(min)}$: these points are indicated as H and L in Figure 1. The values of $\gamma_{max(min)}$ are

$$\gamma_{max} \to 2\gamma_g + 4E_0\gamma_g^2 \tag{8}$$

$$\gamma_{min} \to E_0 + \frac{1}{4E_0} \tag{9}$$

in the limit $\gamma_g \gg 1$.

Orbits close to the O-point describe the motion of deeply trapped electrons. Using that P_z is close to $v_g\gamma_g mc$ and

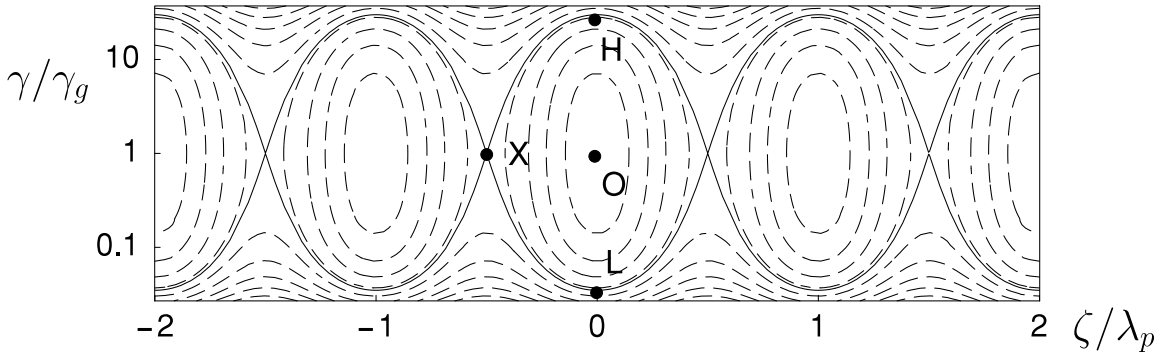

Fig. 1. Phase diagram for $\mathcal{H}_0$ with O-point (O), X-point (X), highest (H) and lowest (L) point of separatrix.

$\zeta \ll \lambda_p$ one finds a harmonic oscillation with synchrotron frequency ω_s

$$\frac{d^2\zeta}{dt^2} + \frac{c^2}{\gamma_g^3}\frac{d^2\Psi}{d\zeta^2}(0)\zeta \equiv \left(\frac{d^2}{dt^2} + \omega_s^2\right)\zeta = 0. \tag{10}$$

Using the wakefield equation, one finds $\omega_s \approx (E_0/\gamma_g^3)^{1/2}\omega_p$, where $\omega_p = k_p c$ denotes the plasma frequency. It is found that $\gamma_g \gg 1$ implies $\omega_s/\omega_p \ll 1$, i.e., for under-dense plasma the motion of deeply trapped electrons in the comoving frame is much slower than the motion of plasma electrons. This justifies a posteriori the quasi-static approximation for the description of the plasma wave.

Once they are accelerated, the electrons eventually propagate faster than the wave, so the energy gain is limited by phase slippage. The acceleration distance is equal to $v_g T$, where T denotes the time during which the electron can remain in the accelerating region (i.e., half a synchrotron period). The maximum acceleration, distance is the *dephasing length* L_d. Since for a large part of the acceleration, the approximation $\gamma \gg \gamma_g$ is valid, the phase slippage can be taken as constant:

$$\frac{d\zeta}{dt} \approx c - v_g \approx \frac{c}{2\gamma_g^2}. \tag{11}$$

With this approximation, one finds $\omega_s \approx \omega_p/2\gamma_g^2$ for the synchrotron frequency of orbits above the separatrix, which indicates that the motion of electrons out-running the wave in the comoving frame is even slower than the motion of deeply trapped electrons. The dephasing length corresponds to a phase slippage distance of half a plasma wavelength, so with Eq. (11) it is found that

$$L_d \approx c\int dt \approx 2\gamma_g^2 \int d\zeta = \lambda_p \gamma_g^2. \tag{12}$$

To illustrate the dynamics further, results of numerical integration of the lowest-order equations of motion are shown in Figure 2. Two different initial conditions inside the separatrix have been chosen: $(\zeta,\gamma) = (-3\lambda_p/20, \gamma_g/5)$, $(-3\lambda_p/10, \gamma_g/5)$ for $E_0 = 1/10$, $\gamma_g = 50$. The time variable is multiplied by v_g to get the acceleration distance L_a, which is expressed as a fraction of the dephasing length. From Figure 2 the approximation of constant phase slippage is seen to hold for a large part of the motion. It fails only during a short time, when the electron rapidly slips backward. This leads to typical sawtooth oscillations for ζ. Orbits near the O-point have a shorter synchrotron oscillation period than orbits close to the separatrix. The maximum energy scales about linearly with the synchrotron period.

3. TRANSVERSE MOTION

In three-dimensional geometry, the wave equation is (Gorbunov & Kirsanov, 1987)

$$\left(k_p^2 + \frac{\partial^2}{\partial\zeta^2}\right)(k_p^2 - \nabla_\perp^2)\Psi = k_p^2(k_p^2 - \nabla_\perp^2)\Phi_p. \tag{13}$$

Assuming that the ponderomotive potential can be written as a product $\Phi_p = \Phi_z(\zeta)\Phi_\perp(\boldsymbol{r}_\perp)$, the solution for Ψ is simply $\Psi = \Psi_z(\zeta)\Phi_\perp(\boldsymbol{r}_\perp)$, where Ψ_z is equal to Ψ in Eq. (7). In this subsection, it is assumed that the laser transverse profile is an axisymmetric Gaussian function $\Phi_\perp(r) = \exp(-r^2/r_0^2)$.

The transverse electron motion follows from the second-order expansion $\mathcal{H} \approx \mathcal{H}_0 + \mathcal{H}_2$ of the Hamiltonian (Eq. 3) with Reitsma (2002)

$$\mathcal{H}_2 = \frac{1}{2m\gamma_0}P_\perp^2 - \frac{1}{2}mc^2\Psi_2 r_\perp^2 \tag{14}$$

where the function Ψ_2 denotes the curvature of the potential Ψ in the vicinity of the propagation axis. The function Ψ_2 is given by

$$\Psi_2(\zeta) = \frac{\partial^2\Psi(r,\zeta)}{\partial r^2}(\zeta, r=0) = -\frac{2E_0}{r_0^2}\cos(k_p\zeta). \tag{15}$$

The transverse forces are focusing in regions with $\Psi_2 < 0 \rightarrow \cos(k_p\zeta) > 0$ and defocusing in regions with $\Psi_2 > 0 \rightarrow \cos(k_p\zeta) < 0$. Only one-fourth of the plasma wavelength is

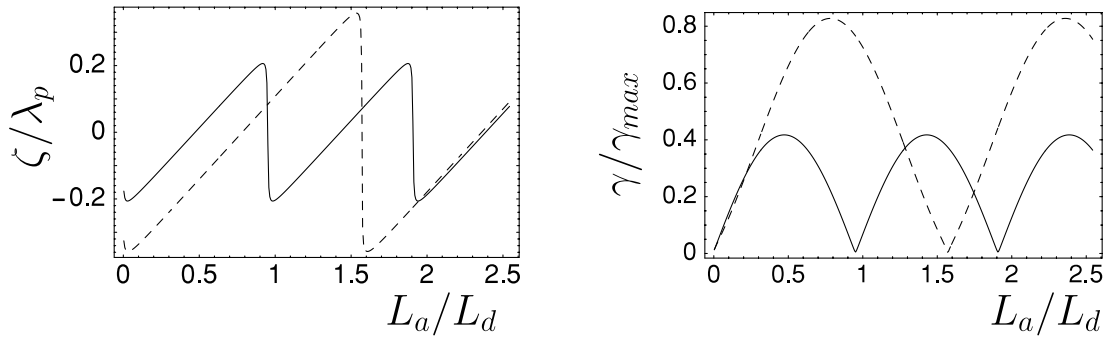

Fig. 2. Phase (left) and energy (right) as functions of acceleration distance for initial conditions $(\zeta,\gamma) = (-3\lambda_p/20, \gamma_g/5)$ (solid lines) and $(\zeta,\gamma) = (-3\lambda_p/10, \gamma_g/5)$ (dashed lines).

both focusing and accelerating, i.e., when $\cos(k_p\zeta) > 0$ and $\sin(k_p\zeta) < 0$. Therefore, the maximum attainable energy γ_{max} and minimum energy γ_{min} for electron trapping are not on the separatrix of Figure 1, but on the orbit through $\zeta = -\lambda_p/4$, $\gamma_0 = \gamma_g$. Their values are given by

$$\gamma_{max} \to 2\gamma_g + 2E_0\gamma_g^2 \tag{16}$$

$$\gamma_{min} \to \frac{1}{2}\left(E_0 + \frac{1}{E_0}\right) \tag{17}$$

in the limit $\gamma_g \gg 1$. In focusing regions, $\mathcal{H}_2$ is the Hamiltonian of a harmonic oscillator with time-dependent mass $\gamma_0 m$ and focusing strength $-\Psi_2$. The time dependence enters through the dependence of γ_0 and Ψ_2 on P_z and ζ, respectively. The transverse oscillations are called *betatron* oscillations. From

$$\omega_\beta^2 = -c^2\,\frac{\Psi_2}{\gamma_0} = \frac{2E_0c^2}{\gamma_0 r_0^2}\cos(k_p\zeta) \tag{18}$$

one finds a condition for the laser pulse width

$$E_0 \ll k_p r_0 \ll \sqrt{\frac{\gamma_g}{E_0}} \tag{19}$$

in order to satisfy $\omega_s \ll \omega_\beta \ll \omega_p$, where $\gamma_{min} < \gamma_0 < \gamma_{max}$ has been used. In this case, the betatron motion is much slower than the motion of plasma electrons, so that the wakefield is correctly described in the quasi-static approximation. Also, the betatron oscillation is much faster than the synchrotron oscillation, so that the (ζ, P_z)-dependence is adiabatically slow and the area α_x in (x, P_x) phase space

$$\alpha_x = \oint P_x\,dx \tag{20}$$

is an adiabatic invariant of the motion (similar for α_y). Note that the requirement that the longitudinal timescale is much longer than the transverse timescale may fail during the rapid backward slip of the electron (see Fig. 2). In this case, there is no adiabatic invariant.

4. COUPLING OF LONGITUDINAL AND TRANSVERSE DYNAMICS

In this section, it is assumed that the time-scales of longitudinal and transverse motion are sufficiently separated, so that the adiabatic invariants α_x and α_y can be defined. Defining x_0, P_{x0} to be the betatron amplitudes for, respectively, x and P_x, one finds that the adiabatic invariant is $\alpha_x = \pi x_0 P_{x0}$ (similar for α_y). The variation of x_0 and P_{x0} due to the evolution of ζ and P_z on the slow time-scale is given by

$$x_0^2 = \frac{\alpha_x}{\pi mc}\sqrt{\frac{-1}{\gamma_0\Psi_2}}, \qquad P_{x0}^2 = \frac{\alpha_x mc}{\pi}\sqrt{-\gamma_0\Psi_2}, \tag{21}$$

which describes the coupling of longitudinal to transverse motion, i.e., adiabatic focusing due to acceleration. To estimate the magnitude of the focusing effect, consider injection with energy $\gamma_i < \gamma_g$ and extraction at energy $\gamma_f > \gamma_g$. The injection phase and the extraction phase are taken as identical, so that the value of Ψ_2 is the same. In this case, the *adiabatic focusing factor*, defined as the ratio of initial to final x_0, equal to the ratio of final to initial P_{x0}, is found to be $(\gamma_f/\gamma_i)^{1/4}$. With Eqs. (16)–(17) it is found that

$$\frac{\gamma_f}{\gamma_i} \le \frac{\gamma_{max}}{\gamma_{min}} \approx (2E_0\gamma_g)^2. \tag{22}$$

For $E_0 = 1/10$, $\gamma_g = 50$, this results in an upper limit of about 3.16 for the focusing factor. Note that acceleration leads to a decrease of opening angle P_{x0}/γ, given by $(\gamma_f/\gamma_i)^{-3/4}$. A plot of the adiabatic focusing factor for $\gamma_g = 50$ is given in Figure 3, where the value of γ_f has been found by taking the zero-order Hamiltonian (Eq. 5) as a constant of the motion.

By rewriting the second-order Hamiltonian $\mathcal{H}_2$ in terms of the adiabatic invariants, one finds the one-dimensional Hamiltonian

$$\mathcal{H}_\alpha = \mathcal{H}_0 + \mathcal{H}_2 = mc^2(\gamma_0 - \Psi_0) - v_g P_z + \frac{\alpha c}{2\pi}\sqrt{\frac{-\Psi_2}{\gamma_0}} \tag{23}$$

that describes the coupling of transverse to longitudinal motion, e.g., the effect of the r-dependence of the accelerating field on the energy gain. The Hamiltonian $\mathcal{H}_\alpha$ depends

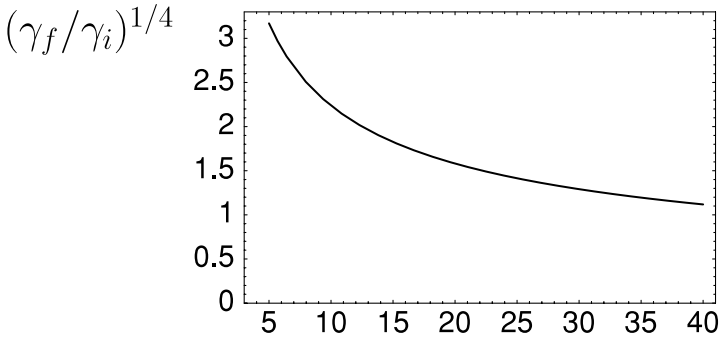

Fig. 3. Adiabatic focusing ratio as a function of initial energy for $\gamma_g = 50$.

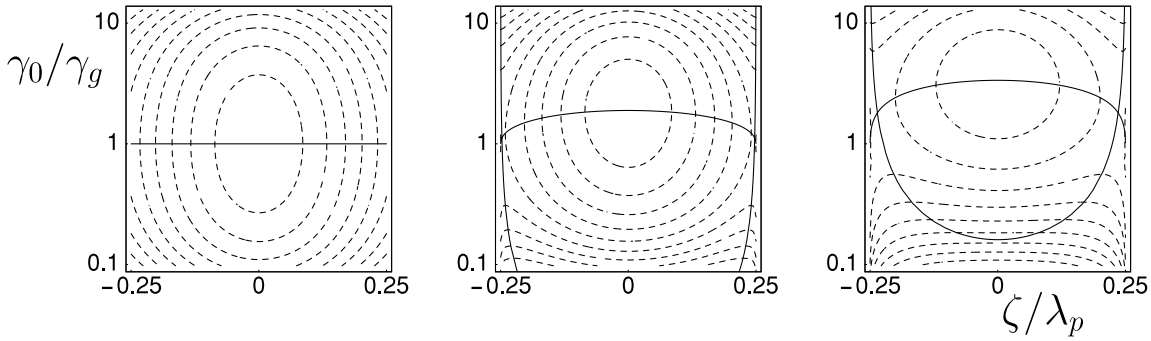

Fig. 4. Phase diagrams for $\mathcal{H}_\alpha$ with $\alpha/\pi r_0 mc = 0$ (left), 1/2 (middle), and 3/2 (right).

on the adiabatic constant $\alpha = \alpha_x + \alpha_y$ and is defined only in the focusing region, where $\Psi_2 < 0$.

The influence of the transverse motion on the longitudinal dynamics is illustrated in Figure 4, which shows phase diagrams of $\mathcal{H}_\alpha$ for $\alpha/\pi r_0 mc = 0$, 1/2, and 3/2. Also indicated are contours of $\partial\mathcal{H}_\alpha/\partial\zeta = 0$ (points of maximum or minimum energy) and $\partial\mathcal{H}_\alpha/\partial P_z = 0$ (turning points). For $\alpha > 0$, energy maxima and minima are found around $\zeta = \pm\lambda_p/4$, which are absent in the case $\alpha = 0$. The turning points, which are always at $\gamma_0 = \gamma_g$ for $\alpha = 0$, are seen to occur at $\gamma_0 \approx \gamma_g(1+\sigma)^{1/2}$, where the approximation $\sigma = (\Psi_0\gamma_g/2)^{1/2}$ $\alpha/\pi r_0 mc \ll \gamma_g^2$ has been used. In Figure 4, X-points are seen to exist near $\zeta = \pm\lambda_p/4$, $\gamma_0 = \gamma_g$. The area inside the separatrix decreases with increasing α in such a way that γ_{min} increases with α and γ_{max} decreases with α.

The influence of transverse motion on longitudinal dynamics is further illustrated in Figure 5. This figure shows one orbit for $\alpha = \pi r_0 mc$ and two orbits for $\alpha = 0$, chosen such that one of them has the same maximum energy and the other one has the same minimum energy. The main difference between the $\alpha = 0$-orbits and the $\alpha > 0$-orbit is seen to be in the low energy ($\gamma_0 < \gamma_g$) part, where the electron with a finite value of α has a larger backward slip in the wakefield.

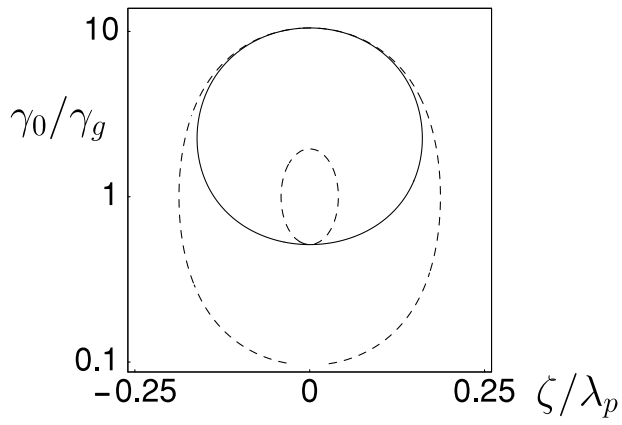

Fig. 5. Selected orbits for $\alpha = 0$ (dashed lines) and $\alpha = \pi r_0 mc$ (solid line).

As a consequence, for a collection of electrons (i.e., a bunch) a finite spread in α effectively leads to bunch length increase and possibly a growth of energy spread. It also means that in the low-energy regime the electron bunch cannot be described as a collection of "slices" labeled by the longitudinal coordinate. In the high energy ($\gamma_0 > \gamma_g$) part, the $\alpha > 0$-orbit is barely different from the large $\alpha = 0$-orbit, indicating that the radial variation of the accelerating field has only little effect on energy gain. This is because the electron moves close to the axis as a result of strong adiabatic focusing during the rapid backward slip—see also Eq. (21).

To check the validity of the paraxial approximation, it is instructive to look at some results of numerical integration of the full equations of motion Eqs. (1)–(2). These simulation results are given in Figure 6, which shows $x_0 P_{x0}$, $\mathcal{H}_\alpha/\mathcal{H}$, x_0, P_{x0}, ζ and γ_0 as functions of the acceleration distance. The following initial conditions have been chosen: $(\zeta, \gamma_0) = (0, \gamma_g/5)$, $(y, P_y) = (0,0)$. For (x, P_x), the cases $(0, mc/2)$ (a) and $(0, mc)$ (b) are compared. The wakefield parameters are $E_0 = 1/10$, $r_0 = \lambda_p$, $\gamma_g = 50$.

The quantity $x_0 P_{x0}$ is seen to be nearly constant for electron a, while there are some fluctuations for electron b. This does not mean that there is not an adiabatic invariant α_x for electron b, it only reflects that $\alpha_x \neq x_0 P_{x0}$. The change of $x_0 P_{x0}$ is most pronounced during the rapid backward slip of electron b, when x_0 reaches its maximum. The behavior of $\mathcal{H}_\alpha/\mathcal{H}$ indicates that the second-order approximation breaks down for electron b. This implies that the parabolic approximation of the focusing potential Ψ is not satisfied, Since $P_{x0} \ll \gamma_0$ during the whole acceleration.

There is a considerable difference in longitudinal dynamics for the two electrons: electron b is seen to slip closer to the defocusing regions $\zeta < -\lambda_p/4$, $\zeta > \lambda_p/4$ and reaches a higher energy than electron a. The influence of phase slippage and acceleration on the betatron motion is seen in the graphs of x_0 and P_{x0} as functions of acceleration distance. The maximum of x_0 is at the point of minimum energy, the maximum of P_{x0} is at the point of maximum energy, indicating that the influence of γ_0 on x_0, P_{x0} dominates over the influence of Ψ_2.

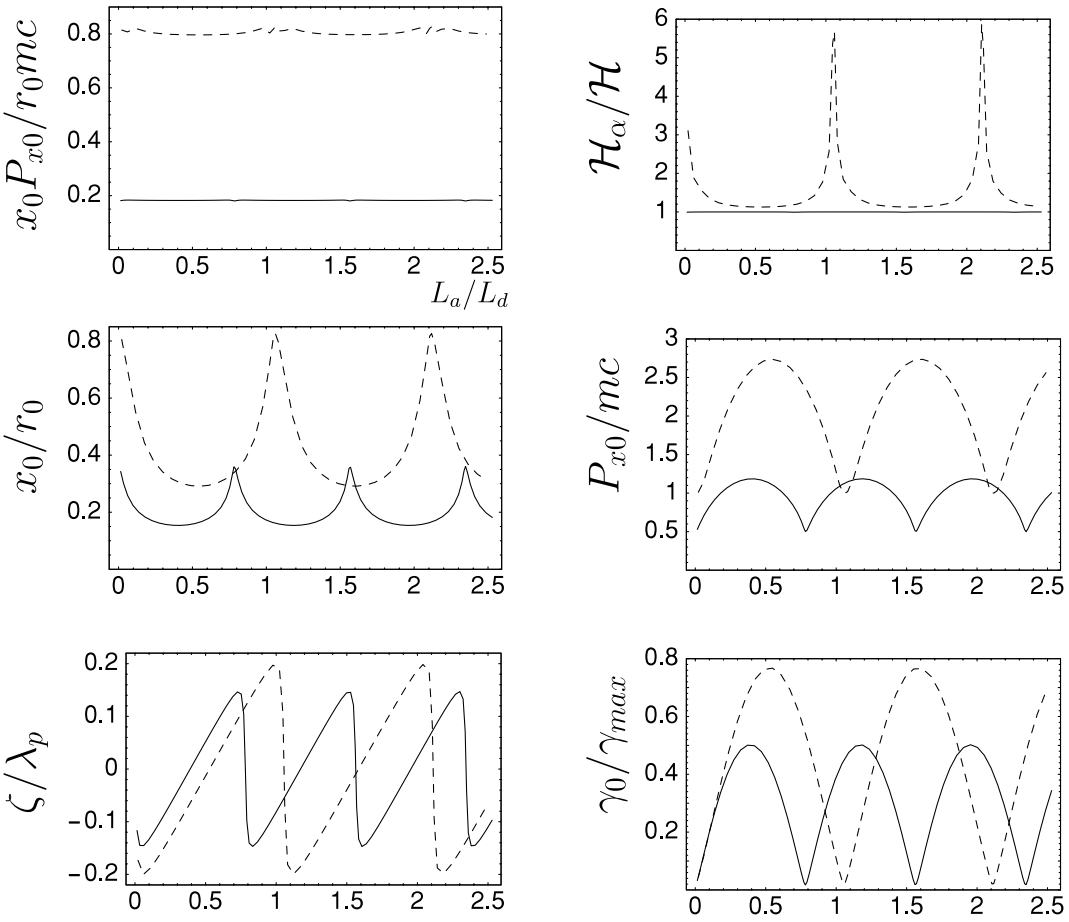

Fig. 6. Simulation results for initial conditions (*a*) $(x, P_x) = (0, mc/2)$ (solid lines) and (*b*) $(x, P_x) = (0, mc)$ (dashed lines) showing influence of betatron oscillation on longitudinal dynamics.

5. CONCLUSIONS

The coupling between longitudinal and transverse electron dynamics described in this article has important consequences for the design of a compact accelerator in which a relatively low energy bunch from a conventional electron source is injected into a single stage of resonant LWFA. From the assumption that the time-scale of the transverse (betatron) oscillation is much shorter than the time-scale of the longitudinal dynamics, we have found that the bunch is adiabatically focused. This focusing effect is strongest at low injection energy and its main consequence is that the longitudinal dynamics becomes close to one-dimensional as soon as the electron's energy has increased above the resonant energy $\gamma_g mc^2$. The influence of the betatron motion on longitudinal dynamics is most important at the injection of the bunch, when the energy is still below the resonant energy. The magnitude of this effect depends on the (largest) value of the adiabatic invariant α, which is determined primarily by the transverse emittance ϵ of the injected electron bunch. As shown in this article, the minimum energy required for trapping in the plasma wave is higher for larger values of α, a spread in α effectively leads to bunch lengthening and growth of energy spread, and the focusing force becomes nonlinear for large values of α. All these results illustrate the importance of having a small transverse emittance for the injected bunch: a small emittance minimizes increase of bunch length and growth of energy spread, and enables focusing to a small spot size to avoid nonlinearities in the focusing force.

REFERENCES Q2

ANDREEV, N.E., GORBUNOV, L.M. & KUZNETSOV, S.V. (1996). *IEEE Trans. Plasma Sci.* **24**, 448.

CHESHKOV, S., TAJIMA, T., HORTON, W. & KOYOKA, K. (2000) *Phys. Rev. ST Accel. Beams* **3**, 071301.

CHIU, C., CHESHKOV, S. & TAJIMA, T. (2000). *Phys. Rev. ST Accel. Beams* **3**, 101301.

ESAREY. E. & PILLOFF, M. (1995) *Phys. Plasmas* **2**, 1432.

Esarey, E., Sprangle, P., Krall, J. & Ting, A. (1996). *IEEE Trans. Plasma Sci.* **24**, 252.

Gorbunov, L.M. & Kirsanov, V.I. (1987). *Sov. Phys. JETP* **66**, 290.

Mora, P. (1992). *J. Appl. Phys.* **71**, 2087.

Mora, P. & Amiranoff, F. (1989). *J. Appl. Phys.* **66**, 3476.

Panofsky, W.H.H. & Wenzel, W.A. (1956). *Rev. Sci. Instrum.* **27**, 976.

Reitsma, A.J.W. (2002). *Electron bunch quality in laser wakefield acceleration*. PhD Thesis. Eindhoven, The Netherlands. http://alexandria.tue.nl/extra2/200212656.pdf

Reitsma, A.J.W., Goloviznin, V.V., Kamp, L.P.J. & Schep, T.J. (2001). *Phys. Rev. E* **63**, 046502.

Tajima, T. & Dawson, J.M. (1979). *Phys. Rev. Lett.* **43**, 267.

Umstadter, D., Chen, S.-Y., Maksimchuk, A., Mourou, G. & Wagner, R. (1996) *Science* **273**, 472